

A novel autoencoder approach to feature extraction with linear separability for high-dimensional data

Jian Zheng¹, Hongchun Qu^{Corresp., 1, 2}, Zhaoni Li¹, Lin Li¹, Xiaoming Tang², Fei Guo²

¹ College of Computer Science and Technology, Chongqing University of Post and Telecommunications, Chongqing, China, China

² College of Automation,, Chongqing University of Posts and Telecommunications,, chongqing, China, China

Corresponding Author: Hongchun Qu
Email address: hcchu@gmail.com

Feature extraction often needs to rely on sufficient information of the input data, however, the distribution of the data upon a high-dimensional space is too sparse to provide sufficient information for feature extraction. Furthermore, high dimensionality of the data also creates trouble for the searching of those features scattered in subspaces. As such, it is a tricky task for feature extraction from the data upon a high-dimensional space. To address this issue, this paper proposes a novel autoencoder method using Mahalanobis distance metric of rescaling transformation. The key idea of the method is that by implementing Mahalanobis distance metric of rescaling transformation, the difference between the reconstructed distribution and the original distribution can be reduced, so as to improve the ability of feature extraction to the autoencoder. Results show that the proposed approach wins the state-of-the-art methods in terms of both the accuracy of feature extraction and the linear separabilities of the extracted features. We indicate that distance metric-based methods are more suitable for extracting those features with linear separabilities from high-dimensional data than feature selection-based methods. In a high-dimensional space, evaluating feature similarity is relatively easier than evaluating feature importance, so that distance metric methods by evaluating feature similarity gain advantages over feature selection methods by assessing feature importance for feature extraction, while evaluating feature importance is more computationally efficient than evaluating feature similarity.

1 A novel autoencoder approach to feature extraction with 2 linear separability for high-dimensional data

3

4

5 Jian Zheng ¹, Hongchun Qu^{1,2,*}, Zhaoni Li ^{1,3}, Lin Li¹, Xiaoming Tang ², Fei Guo²

6

7 ¹ College of Computer Science and Technology, Chongqing University of Posts and
8 Telecommunications, Chongqing, 400065, China9 ² College of Automation, Chongqing University of Posts and Telecommunications, Chongqing,
10 400065, China

11

12

13 Corresponding Author:

14 Hongchun Qu

15 Congwenlu Road, Chongqing, 400065, China

16 Email address: hcchu@gmail.com

17

18

19 Abstract

20 Feature extraction often needs to rely on sufficient information of the input data, however, the distribution
21 of the data upon a high-dimensional space is too sparse to provide sufficient information for feature
22 extraction. Furthermore, high dimensionality of the data also creates trouble for the searching of those
23 features scattered in subspaces. As such, it is a tricky task for feature extraction from the data upon a
24 high-dimensional space. To address this issue, this paper proposes a novel autoencoder method using
25 Mahalanobis distance metric of rescaling transformation. The key idea of the method is that by
26 implementing Mahalanobis distance metric of rescaling transformation, the difference between the
27 reconstructed distribution and the original distribution can be reduced, so as to improve the ability of
28 feature extraction to the autoencoder. Results show that the proposed approach wins the state-of-the-art
29 methods in terms of both the accuracy of feature extraction and the linear separabilities of the extracted
30 features. We indicate that distance metric-based methods are more suitable for extracting those features
31 with linear separabilities from high-dimensional data than feature selection-based methods. In a high-
32 dimensional space, evaluating feature similarity is relatively easier than evaluating feature importance, so
33 that distance metric methods by evaluating feature similarity gain advantages over feature selection
34 methods by assessing feature importance for feature extraction, while evaluating feature importance is
35 more computationally efficient than evaluating feature similarity.

36

37 Keyword: Autoencoder, Distance metric, Feature extraction

38

39 Introduction

40 High-dimensional data usually contains rich features, through extracting the important features,
41 those irrelevant attributes in high-dimensional data can be filtered, thereby achieving data

42 dimensionality reduction (*Xue et al., 2015*). Hence, feature extraction is considered to be one of
43 the important methods for data dimension reduction (*Bo et al., 2016*).

44 Feature extraction is a hot topic in recent years, aiming to gain the most valuable features from
45 the input data (*H.Tao et al., 2016; M. Luo et al., 2018*). High dimensionality of data, the so-
46 called the curse of dimensionality, brings negative effects for feature extraction (*J.Gui et al.,*
47 *2018; R. Chakraborty, N.R.Pal, 2015*). Upon a low-dimensional space, those relations between
48 the data are relatively compact but they may become sparse upon a high-dimensional space (*Bing*
49 *et al., 2021*), e.g., the data space with more than 10 dimensionalities (*A.-M., et al, 2011*). Clearly,
50 sparse relations between data are usually considered to be an unfavorable factor for feature
51 extraction since feature extraction needs to rely on the relations between data (*Bo et al., 2021*).
52 Beyond that, those latent features scattered in subspaces inside a high-dimensional space not
53 only inspect the ability of methods to extract features (*L. Wang et al., 2016*), but also test their
54 extraction efficiency. Hence, it is a challenge for feature extraction from high-dimensional data.

55 Recently, some opinions have been proposed for feature extraction, for instance, distance
56 metric-based methods, where, the typical representative is the well-known Mahalanobis distance-
57 based methods, which evaluates the similarity between samples using the covariance matrix of
58 data (*R. De et al, 2000*). Furthermore, *S.-Y (2018)* et al proposed the intrinsic semi-supervised
59 metric learning (ISSML) based on a distance metric for feature extraction. Similar, the methods
60 implemented in (*P. Zadeh et al, 2016*) and (*H. Luo, 2017*) also applied distance metrics.
61 Certainly, also including, the information-theoretic metric learning is (ITML) (*J. Mei et al, 2014*)
62 employed a distance metric to obtain features. These methods in (*S. Ying et al, 2018; P. Zadeh et*
63 *al, 2016; H. Luo, 2017; J. Mei et al, 2014*) address the issues of symmetric positive-definite
64 matrix minimization during feature extraction, but there are several problems in them, 1) since
65 most of them use iterative calculation while performing feature selection, optimization issues
66 have to be addressed iteratively. 2) Most of them need to rely on parameter selection to obtain
67 those desired features. Usually, feature selection-based methods are also considered to be used
68 for feature extraction. Such methods achieve feature extraction through analyzing the
69 information of feature subsets, for example, the cheap feature selection method based on *k*-
70 means algorithm (*Marco et al, 2021*) selects the *m* features with the highest relevance measure
71 through obtaining a clustering for each subset of features. Although the method (*Marco et al,*
72 *2021*) is a novel measurement for feature relevance, which is beneficial for feature selection,
73 however, calculating per subset of features needs to spend a lot time cost. In order to reduce the
74 correlation between features, some measurements for quickly assessing features are proposed,
75 e.g., the information entropy metric (*T. X. et al, 2019*), whereas the method (*T. X. et al, 2019*) has
76 a bias toward features, which may result in appearing selecting deviation during feature
77 extraction. Another kind of feature selection method depends on eigen decomposition, such as,
78 locally linear embedding (LLE) (*R. Hettiarachchi, J. F. Peters, 2015; Ugochukwu Ejike Akpudo,*
79 *Jang-Wook Hur, 2020*), multi-manifold discriminant isometric feature mapping (MMD-
80 ISOMAP) (*Bo.Y et al, 2016*), ISOMAP-KL (*Alaor Cervati Neto, Alexandre L. M. Levada, 2020*),
81 however, they cannot assess the importance of the features in the background space explicitly.

82 Neural network-based methods are favored because of excellent feature capture ability
83 (*Hong.C et al, 2022*), e.g., Multilayer Perceptron Neural Network (*K. Sun et al., 2017*). For
84 dimension reduction, feature extraction and data compression, autoencoder-based networks
85 provide an interpretable approach for the unknown meaningful insights (*Ang et al., 2017*) by
86 learning non-identity mapping functions (*Jian et al., 2022*), for instance, *Rami et al (2022)*
87 developed interpretable data representation for data dimensionality reduction using Logic-
88 Oriented and Granular Logic Autoencoders, and such as, Autoencoder (*Angshul Majumdar,*
89 *2019*) for image compression, and Blind Denoising autoencoder (*Fei et al, 2020*) for denoising.
90 In addition, sparse autoencoders are used as an unsupervised feature extractor to serve data
91 dimensionality reduction, feature extraction and data mining (*Z.Qiang et al., 2018*), e.g., *K.-J et*
92 *al (2018)* proposed Sparse Autoencoder (SAE) for feature extraction of ferroresonance
93 overvoltage waveforms in power distribution systems. *Yan et al (2018)* used Stacked Sparse
94 Autoencoder (SSAE) to extract effective features. In addition, the Autoencoders (*Qu et al., 2021,*
95 *Qu et al., 2020, Jian et al., 2022*) also successfully capture the low-dimensional features from
96 high-dimensional data, however, these captured low-dimensional features do not show good
97 linear separability. In terms of addressing high-dimensional complex problems, deep methods
98 are the state-of-the-art solution in many disciplines (*R.Abadía, et al, 2022*), e.g., video and
99 language processing, etc.

100 In this study, our motivation is to extract the features with linear separabilities from the data in
101 a high-dimensional space. Thus, we proposed a novel autoencoder method based on Mahalanobis
102 distance metric of rescaling transformation. The proposed method does not have to address any
103 optimization issue, and also it can focus on the whole data distribution.

104 We summarize the main contributions of this work as follows:

105 (i) Distance metric-based methods are more suitable for extracting those features with linear
106 separabilities from high-dimensional data than feature selection-based methods.

107 (ii) Assessing feature similarity in a high-dimensional space is relatively easier than evaluating
108 feature importance, therefore, distance metric approaches by evaluating feature similarity have
109 more advantages than feature selection approaches by evaluating feature importance in terms of
110 feature extraction.

111 (iii) The computational time of distance metric-based algorithms is higher than that of feature
112 selection-based algorithms upon a high-dimensional space.

113 This paper is organized as follows. Section 2 describes the proposed method and implements
114 the proposed model, including training for the model and parameter configuration. Experiment
115 datasets, competing methods, and experiment description are given in Section 3. Section 4
116 presents experiment results. Section 5 draws conclusions.

117

118 **Methods**

119 **Theory**

120 Given a sample $X = \{x_i | 1 \leq i \leq N\}$, and $X \subseteq \mathfrak{R}^d$. \mathfrak{R}^d is the d -dimensional Euclidean space. P is the
121 probability distribution of X , denoted as original probability distribution. $u(X)$ and Γ_x are the

122 mean vector and the covariance matrix of X , respectively. Let us assume that $Z = \{z_j | 1 \leq j \leq N\}$ is
 123 the reconstructed X , and $Z \subseteq \mathfrak{R}^d$. Q is the probability distribution of Z , denoted as approximate
 124 probability distribution. Similar, $u(Z)$ and Γ_z are the mean vector and the covariance matrix of Z ,
 125 respectively. The K-L divergence (D. Tao et al, 2009) between the two distributions P and Q is
 126 given in Eq. (1).

$$127 \quad K(P \parallel Q) = \frac{1}{2} \left[\log |\Gamma_z| - \log |\Gamma_x| + \text{tr}(\Gamma_z^{-1} \Gamma_x) + \text{tr}(\Gamma_z^{-1} D_{xz}) \right] \quad (1)$$

128 Where $|\Gamma| = \det(\Gamma)$. The $\text{tr}(\cdot)$ is the trace of a matrix. $D_{xz} = (u(X) - u(Z))(u(X) - u(Z))^T$ is a symmetrical
 129 matrix. Training a distance metric is equivalent to finding a rescaling of a sample which replaces
 130 each x_i with $M^T x_i$ (Lin et al, 2019), so the K-L divergence in Eq. (1) can be converted into Eq.
 131 (2), having

$$132 \quad K_L^*(P \parallel Q) = \frac{1}{2} \left[\log |M^T \Gamma_z M| - \log |M^T \Gamma_x M| + \text{tr} \left((M^T \Gamma_z M)^{-1} (M^T (\Gamma_x + D_{xz}) M) \right) \right] \quad (2)$$

133 Where M is a metric matrix and satisfies $A^* = MM^T$, and $M \in \mathfrak{R}^{d \times d_0}$, $d_0 \leq d$. The K-L divergence in
 134 Eq. (2) is the rescaling transformation for the K-L divergence in Eq. (1) using the distance metric
 135 matrix A^* . To reduce the difference between the approximate distribution Q and the original
 136 distribution P , we consider Mahalanobis distance metric for K-L divergence in Eq. (2), having

$$137 \quad K-L(d_{A^*}) = K_L^*(P \parallel Q) + \sum_{1 \leq i, j} d_{A^*}(x_i, z_j) \quad (3)$$

138 $d_{A^*}(x_i, z_j)$ is Mahalanobis distance between x_i and z_j using A^* . The advantage of doing this is that
 139 the Mahalanobis distance using A^* can appropriately measure similarities between the input
 140 sample and the reconstructed input sample because of non-negativity (i.e., $d_{A^*}(x_i, z_j) \geq 0$),
 141 distinguishability (i.e., $d_{A^*}(x_i, z_j) = 0 \Leftrightarrow x_i = z_j$) and symmetry (i.e., $d_{A^*}(x_i, z_j) = d_{A^*}(z_j, x_i)$) (Lin et al,
 142 2019). Eq. (4) gives the calculation of $d_{A^*}(x_i, z_j)$, where A^* can be decomposed as $A^* = MM^T$.

$$143 \quad d_{A^*}(x_i, z_j) = \sqrt{(x_i - z_j)^T A^* (x_i - z_j)} \quad (4)$$

144

145 Model implementation

146 A classic auto encoder (AE) consists of an input layer, a hidden-layer and an output layer. For
 147 AE, the loss error is often measured by using the distance between the original input instance, the
 148 predicted instances, and the reconstructed instance (L. Theis et al, 2017). Usually, using
 149 divergence metrics or expanding autoencoder structures (e.g., enlarging the number of hidden
 150 layers) is more helpful for autoencoders to characterize the data distribution and to learn the
 151 desired representations (Weining et al, 2017). As such, we designed an autoencoder with
 152 multiple-hidden layers, namely m -AE, and $m \geq 1$, as shown in Fig.1. In addition, the K-L
 153 divergence in Eq. (3) was used to increase the ability of m -AE to capture low-dimensional
 154 feature representations. The loss error $\nabla_{KL}(\mathbf{w}, \mathbf{b})$ in m -AE is given as follows:

$$155 \quad \nabla_{KL}(\mathbf{w}, \mathbf{b}) = \sum \|e_X - e_Z\|^2 + K-L(d_{A^*}) \quad (5)$$

156 Where e_x, e_z are the inputting and the reconstructed inputting, respectively. $\nabla_{KL}(\mathbf{w}, \mathbf{b})$ is updated
157 through using the backpropagation manner.

158 To better train the proposed model, we carefully studied part hyper parameters in the model.
159 For the rest of hyper parameters, their default values were used.

160 (i) Optimizer. Common optimizers are Adam, RMSprop, SGD, Momentum, Nesterov, etc.
161 However, we selected Adam as the optimizer of m-AE, since Adam has the ability to handle
162 sparse gradients (Diederik P. Kingma, Jimmy Lei Ba, 2015). Compared with other optimizers,
163 Adam is more suitable for high-dimensional data. Moreover, Adam can provide different
164 adaptive learning rates for different hyper parameters.

165 (ii) Activation function. Gradient vanishing is easily to be induced during passing gradients
166 backwards for neural networks, in this case, the probability of gradient vanishing caused by
167 activation function Sigmoid is relatively high. Similar to Sigmoid, activation function tanh also
168 suffers from this problem. While for activation function ReLu, the phenomenon of gradient
169 vanishing is partially alleviated, meaning that gradient vanishing does not appear in the positive
170 interval of ReLu. Furthermore, ReLu converges much faster than Sigmoid and Tanh. Therefore,
171 we chose ReLu as the activation function of m-AE.

172 (iii) Iteration epoch. We dynamically adjust the iteration epoch according to training accuracy.
173 For instance, when training accuracy starts to change from large to small, we reduce iteration
174 epoch in order to prevent over-fitting. When the difference in accuracy between training and
175 testing is minimal, the current iteration epoch can be accepted and training procedure is stopped.

176 We give the training algorithm for m-AE in Algorithm 1. In the algorithm, the training set
177 $Train_set$ is divided into two datasets $TCro_train, TCro_val$ in step 1. Since m-AE has multiple hidden
178 layers, we set m in the range of O_m , in order to determine the m , the dataset $TCro_train$ is used to
179 train m-AE. The data set $TCro_val$ is used for the validation of the network structure of m-AE. To
180 get the optimal m , denoted as m_{opt} , the cross-validation is implemented in step 2 to step 18,
181 where the procedure of step 6 and step 10 describes the calculation process of loss error $\nabla_{KL}(\mathbf{w}, \mathbf{b})$.
182 After gaining the optimal m , m-AE is trained using the training set $Train_set$. Using
183 backpropagation manner updates network parameters until m-AE can converge, as shown in step
184 18 to step 28. The procedure shown in step 29 to step 33 indicates that the maximum training
185 accuracy $Train_acc$ are outputted and the well trained m-AE is saved.

186

187 **Algorithm 1.** Training for m-AE.

188 Input: Training set $Train_set, A^* = I \in \mathbb{R}^{d \times d}$ is an identity matrix, iteration epoch T, L , parameter
189 O_m .

190 Output: Training accuracy $Train_acc$.

191 **Begin:**

192 1. $Train_set$ is divided into $TCro_train, TCro_val$;

193 2. **for** $t=1$ to T **do:**

194 3. **foreach** m in O_m :

195 4. Decompose A^* as satisfying $A^* = MM^T$ using eigen decomposition.

196 5. Calculate loss error $\nabla_{KL}(\mathbf{w}, \mathbf{b})$ using Eq. (5) and the procedure is summarized as
 197 following:
 198 6. The procedure:
 199 7. Calculate $K_L^*(P \parallel Q)$ using Eq. (2).
 200 8. Calculate $d_{A^*}(x_i, z_j)$ using Eq. (4).
 201 9. Take $K_L^*(P \parallel Q)$ and $d_{A^*}(x_i, z_j)$ into Eq. (3) to calculate $K-L(d_{A^*})$.
 202 10. For any x_i, x_j , calculate $\nabla_{KL}(\mathbf{w}, \mathbf{b})$ using Eq. (5).
 203 11. Calculate training accuracy $T_acc = m\text{-AE}(T^{Cro_train}, m; t)$;
 204 12. Validate m-AE using data set T^{Cro_val} ;
 205 13. Calculate validation accuracy $V_acc = m\text{-AE}(T^{Cro_val}, m; t)$
 206 14. Update weight $\mathbf{w} \leftarrow \mathbf{w} + \nabla \mathbf{w}$.
 207 15. Update A^* as MM^T .
 208 16. Until A^* and hyper parameters converge.
 209 17. **end foreach**
 210 18. **end for**
 211 19. Get the optimal value of m , i.e., $m_{opt} = \arg \max(V_acc)$;
 212 20. **for** $l=1$ to L **do**:
 213 21. Decompose A^* as satisfying $A^* = MM^T$ using eigen decomposition.
 214 22. Train m-AE using training set $Train_set$ and m_{opt} ;
 215 23. Update network parameters using the optimizer Adam ;
 216 24. Calculate loss error $\nabla_{KL}(\mathbf{w}, \mathbf{b})$ using Eq. (5);
 217 25. Calculate training accuracy $Training_acc(l) = m\text{-AE}(Train_set; m_{opt})$;
 218 26. Update A^* as MM^T ;
 219 27. Using backpropagation manner updates network parameters;
 220 28. **end for**
 221 29. Select the l so that $l_{max} = \arg \max(Training_acc(l))$;
 222 30. Get the maximum training accuracy $Train_acc$ in the l_{max} -th iteration ;
 223 31. $Train_acc = m\text{-AE}(Train_set; m_{opt}, l_{max})$;
 224 32. Output $Train_acc$
 225 33. Save the well trained m-AE($Train_set; m_{opt}, l_{max}$);
 226 **End**
 227

228 EXPERMENTS

229 Datasets and assessment metrics

230 To verify the performance of the proposed m-AE, we selected 4 benchmark datasets with
 231 different data dimensions from the UCI machine learning repository (*C. L. Blake, C. J. Merz,*
 232 *1998*). The attributes of the 4 benchmark datasets are summarized in Table 1.

233 Receiver operating characteristic curve (ROC) and corresponding area under curve (AUC) are
234 usually used to assess the precision of machine learning methods. Therefore, AUC is taken as the
235 assessment metric of method precision.

236

237 **Competing and benchmark methods**

238 Since m-AE applies the distance metric of rescaling transformation, the methods based on a
239 distance metric were used for comparisons, including ISSML (*S.-Y et al, 2018*) and ITML (*J.
240 Mei et al, 2014*). Certainly, the method based on feature selection was also considered, i.e.,
241 MMD-ISOMAP (*Bo.Y et al, 2016*). In addition, autoencoder-based approaches were used as a
242 comparison, e.g., the SAE (*K.-J et al, 2018*). Furthermore, to further examine the effects of the
243 distance metric of rescaling transformation on the performance of m-AE, a benchmark model
244 was developed with m-AE as a reference. The developed benchmark model used the same
245 structure and parameter configuration of m-AE without using the distance metric of rescaling
246 transformation, namely AE-BK.

247 We implemented the corresponding algorithms of the six models using Python on Tensorflow
248 framework. While for those parameters of competing methods, we adopted those values
249 observed in the corresponding literature. Certainly, unless otherwise stated, the five
250 corresponding algorithms all run on the same GPU and apply the same experimental
251 configuration settings.

252

253 **Experiment description**

254 Experiments were conducted on the four benchmark datasets in order to validate the ability of
255 these six models to extract features and their efficiency.

256 **Experiment I.** To test the robustness of m-AE. The proposed m-AE has multiple hidden
257 layers, since the number of hidden layers (i.e., the m) significantly affects the precision of feature
258 extraction, the m needs to be firstly verified, i.e., robustness testing of the model, let m set in the
259 range of $\{1, 2, 3, 4, 5, 7, 10, 15, 20\}$.

260 **Experiment II.** To test the ability of feature extraction for the six models. The six models
261 were run on the four benchmark datasets, and then the testing results were analyzed.

262 **Experiment III.** To compare the efficiency of our method with competing methods. These
263 methods were performed on four benchmark datasets and observed their running time.

264 **Ablation experiments.** To verify that using the distance metric of rescaling transformation
265 can be beneficial for extracting linearly separable features, the ablation experiments were also
266 designed.

267 In addition, to eliminate randomness during the experiment and present an objective result,
268 we used cross-validation to verify the six models. We randomly selected two datasets from the
269 four benchmark datasets as the training set to train the six models. Once the six models were well
270 trained, they were tested on the four benchmark datasets, respectively. The process was repeated
271 five times, independently, then we took the average of five testing results as a measurement.

272

273 RESULTS

274 Experiments on robustness

275 Results in Fig.2 show that the performance of the proposed m-AE and the benchmark model AE-
276 BK improves along with increasing of m , and then the performance remains stable when m
277 reaches a certain size, i.e., $m=3$. This means that m-AE and AE-BK are not sensitive to large m
278 on the four benchmark datasets, i.e., their network structures are robust within a reasonable
279 range. Therefore, let m be equal to 3 in subsequent experiments.

280

281 Comparisons of accuracy extraction

282 Results in Table 2 show that the proposed m-AE wins the four competing models and the
283 benchmark model in the accuracy of feature extraction on all considered instances. For
284 competitors, ISSML, ITML and SAE outperform MMD-ISOMAP in most benchmark datasets
285 for the extracted accuracy.

286

287 Comparisons of linear separability.

288 The results of ablation experiments in Fig.3 (a) show that compared with the models without
289 using distance metrics, e.g., AE-BK, SAE, the models using distance metrics (including m-AE,
290 ISSML, ITML) perform much better on most datasets in the extracted accuracy of the features
291 with linear separabilities. Similar, the models using distance metrics also win the model using
292 feature selection, as shown in Fig.3 (b). To observe the linear separabilities of the extracted
293 features from the four benchmark datasets, we projected these extracted features onto 2-
294 dimensional space, and then visualized them. Fig.4 displays the results of visualized distribution
295 on the four benchmark datasets by the six models. The visualized results show that it is optimal
296 for the separation distance between different types of features extracted by m-AE, meaning that
297 compared with competing and benchmark models, m-AE is a winner in terms of the linear
298 separabilities of the extracted features. Together, these results imply that distance metric-based
299 methods have advantages over feature selection-based methods in terms of extracting the
300 features with linear separabilities.

301

302 Running time

303 Fig.5 displays the running time of methods. Obviously, the advantage of m-AE in running time is
304 not as significant as that in both the extracted accuracy and the linear separabilities of the
305 extracted features. MMD-ISOMAP spends less in running time on most benchmark datasets than
306 distance metric-based methods, meaning that the execution efficiency of feature selection-based
307 methods is higher than that of distance metric-based methods when running upon a high-
308 dimensional space. Distance metric-based methods take a lot of time to calculate the distance
309 between each point pair upon a high-dimensional space, so as to increase the running time.

310

311 Discussion

312 **Insights gained from investigation**

313 Compared with the competitors, the proposed m-AE has outstanding advantage in term of both
314 the accuracy of feature extraction and the linear separabilities of the extracted features on high-
315 dimensional data. We interpret it as following. On one hand, Mahalanobis distance in Eq. (3)
316 can appropriately measure similarities between the input sample and the reconstructed input
317 sample, so as to minimize the loss error of m-AE in Eq. (5). As such, m-AE gains the desired
318 accuracy of feature extraction. On the other hand, we performed a rescaling on K-L divergence
319 metric in Eq. (2) by using A^* in Eq. (4), which effectively allows the extracted features to present
320 linear separabilities, because the rescaling can maximized the classification distance between the
321 extracted different types of features. Hence, the features extracted by m-AE present linear
322 separabilities than competitors .Overall, m-AE outperforms the competitors in extracted accuracy
323 and the linear separabilities of the extracted features.

324 In a high-dimensional space, distance metric-based methods easily evaluates the feature
325 similarity by calculating the distance between the data, however, feature selection-based methods
326 relatively difficulty assess the feature importance. Therefore, distance metric-based methods, e.g.,
327 ISSML (*S.-Y et al, 2018*) and ITML (*J. Mei et al, 2014*), are more suitable for extracting those
328 low-dimensional features with the linear separability from high-dimensional data than feature
329 selection-based methods. However, the computational time of feature selection-based methods,
330 e.g., MMD-ISOMAP (*Bo.Y et al, 2016*), is lower than that of distance metric-based methods in a
331 high-dimensional space, since distance metric-based methods spend too much in calculating the
332 distance between each point pair.

333 Although autoencoders have excellent feature capture capabilities, they may perform poorly in
334 extracting linearly separable features, e.g., SAE (*K.-J et al, 2018*). Whereas, this deficiency of
335 autoencoders can be remedied by introducing a distance metric. Certainly, there are many
336 methods of distance metrics, e.g., Wasserstein distance metric (*Na et al, 2019; Jian et al, 2022*),
337 Bhattacharyya distance metric (*Mariucci E, Reiß M, 2017*).

338

339 **Limitations**

340 The ability of the autoencoder to extract linearly separable features depends on the
341 reconstructed data distribution, while the reconstruction of the data distribution is achieved by
342 the Mahalanobis distance metric of rescaling transformation. Upon a high-dimensional space, the
343 calculation of Mahalanobis distance metric is relatively complicated than that up a low-
344 dimensional space. Moreover, matrix factorization operation needs to be implemented for each
345 computation, therefore, the proposed model is trained using large-scale high-dimensional data
346 until it can converge, which may take longer training epoch.

347

348 **Conclusions**

349 This paper proposed a novel autoencoder method using Mahalanobis distance metric of
350 rescaling transformation to extract linearly separable features from the data in the high-
351 dimensional space. The difference between the reconstructed distribution and the original

352 distribution can be reduced by implementing Mahalanobis distance metric of rescaling
353 transformation, so that the autoencoder can extract the desired features. Finally, results on real
354 high-dimensional datasets show compared with competing methods, the proposed method is a
355 winner in both the accuracy of feature extraction and the linear separabilities of the extracted
356 features. We find that the linear separabilities of those features obtained by the distance metric-
357 based methods are better than that of obtained by the feature selection-based methods. Upon a
358 high-dimensional space, since evaluating feature similarity is relatively easier than evaluating
359 feature importance, distance metric-based methods have more advantages than feature selection-
360 based methods for linearly separable feature extraction, however, feature selection-based
361 methods are better than distance metric-based methods in computational efficiency. In future
362 work, we will look at exploring low-dimensional feature extraction from high-dimensional data
363 under noise disturbance.

364

365 **Funding**

366 The funding received from the National Natural Science Foundation of China under grant
367 #61871061

368

369 **Competing interests**

370 The authors declare no conflict of interest.

371

372 **References**

- 373 **Alaor Cervati Neto, Alexandre L. M. Levada. 2020.** ISOMAP-KL: a parametric approach for
374 unsupervised metric learning. *2020 33rd SIBGRAPI Conference on Graphics, Patterns and*
375 *Images (SIBGRAPI)*. 1-1.
- 376 **A.-M. Zhou, K. D. Kumar, Z.-G, Hou. 2011.** Finite-time attitude tracking control for
377 spacecraft using terminal sliding mode and Chebyshev neural network. *IEEE Trans. Syst.,*
378 *Man, Cybern. B, Cybern.* **41(4)**:950-963.
- 379 **Ang Jun Chin, Andri Mirzal, Habibollah Haron. 2016.** Supervised, Unsupervised and Semi-
380 supervised Feature Selection: A Review on Gene Selection. *IEEE Transactions on*
381 *Computational Biology and Bioinformatics* **13(5)**:971-989
- 382 **Angshul Majumdar. 2019.** Blind Denoising Autoencoder. *IEEE Transactions on Neural*
383 *Networks and Learning Systems* **30(1)**:312-317.
- 384 **Binghao Yan, Guodong Han. 2018.** Effective Feature Extraction via Stacked Sparse
385 Autoencoder to Improve Intrusion Detection System. *IEEE Access* **6**:41238-41248.
- 386 **Bing Tu, Xiaolong Liao, Chengle Zhou. 2021.** Feature Extraction Using Multitask Superpixel
387 Auxiliary Learning for Hyperspectral Classification. *IEEE Transactions on Instrumentation*
388 *and Measurement* **70**:1-16.
- 389 **Bo Peng, Shuting Wan, Ying Bi. 2021.** Automatic Feature Extraction and Construction Using
390 Genetic Programming for Rotating Machinery Fault Diagnosis. *IEEE Transactions on*
391 *Cybernetics* **51(10)**:4909-4923

- 392 **Bo Tang, Steven Kay, Haibo He. 2016.** Toward Optimal Feature Selection in Naive Bayes for
393 Text Categorization. *IEEE Transactions on Knowledge and Data Engineering* **28(9)**:2508-
394 2521.
- 395 **Bo. Yang, M. Xiang, Y. Zhang. 2016.** Multi-manifold discriminant isomap for visualization and
396 classification. *Pattern Recognition* **55**:215-230.
- 397 **C. L. Blake and C. J. Merz. 1998.** UCI Repository of Machine Learning Databases,
398 Department of Information and Computer Science. [Online]. Available: <http://www.ics.uci.edu/mllearn/MLRepository.html>
399
- 400 **Diederik P. Kingma, Jimmy Lei Ba. 2015.** Adam: A method for stochastic optimization. arXiv
401 preprint. arXiv:1412.6980v8.
- 402 **D. Tao, X. Li, X. Wu, S. J. Maybank. 2009.** Geometric mean for subspace selection. *IEEE*
403 *Transactions on Pattern Analysis and Machine Intelligence* **31(2)**:260-274.
- 404 **Fei Yang, Luis Herranz, Joost van de Weijer. 2020.** Variable Rate Deep Image Compression
405 With Modulated Autoencoder. *IEEE Signal Processing Letters* **27**:331-335.
- 406 **H. Luo. 2017.** Hyperspectral image classification using metric learning in one-dimensional
407 embedding framework. *IEEE J. Sel. Topics Appl. Earth Observ. Remote Sens.* **10(5)**:1987-
408 2001.
- 409 **Hongchun Qu, Jian Zheng, Xiaoming Tang. 2022.** Effects of loss function and data sparsity
410 on smooth manifold extraction with deep model. *Expert Systems With Applications* **190**:1-
411 10.
- 412 **Hongchun Qu, Lin Li, Zhaoni Li, Jian Zheng. 2021.** Supervised discriminant Isomap with
413 maximum margin graph regularization for dimensionality. *Expert Systems With*
414 *Applications* **180**:1-14.
- 415 **H. Tao, C. Hou, F. Nie. 2016.** Effective Discriminative Feature Selection With Nontrivial
416 Solution. *IEEE Transactions Neural Network Learning System* **27(4)**:796-808.
- 417 **J. Gui, Z. Sun, S. Ji. 2018.** Feature Selection Based on Structured Sparsity: A Comprehensive
418 Study. *IEEE Transactions Neural Network Learning System* **28 (7)**:1490-1507.
- 419 **Jian Zheng, Hongchun Qu, Zhaoni Li, Lin Li, Xiaoming Tang. 2022.** An irrelevant attributes
420 resistant approach to anomaly detection in high-dimensional space using a deep hyper
421 sphere structure. *Applied Soft Computing* **116** :1-20.
- 422 **J. Mei, M. Liu, H. R. Karimi. 2014.** Logdet divergence-based metric learning with triplet
423 constraints and its applications. *IEEE Transaction Image Process.* **23(11)**:4920-4931.
- 424 **K. Sun, S. H. Huang, D. S. Wong. 2017.** Design and Application of a Variable Selection
425 Method for Multilayer Perceptron Neural Network With LASSO. *IEEE Transactions*
426 *Neural Networks Learning System* **28(6)**:1386-1396.
- 427 **Kunjin Chen, Jun Hu, Jinliang He. 2018.** A Framework for Automatically Extracting
428 Overvoltage Features Based on Sparse Autoencoder. *IEEE Transactions on Smart Grid*
429 **9(2)**:594-604.

- 430 **Lin Feng, Huibing Wang, Bo Jin. 2019.** Learning a Distance Metric by Balancing KL-
431 Divergence for Imbalanced Datasets. *IEEE Transactions on Systems, Man, and*
432 *Cybernetics: Systems* **49(12)**:2384-2395.
- 433 **L. Theis, W. Shi, A. Cunningham. 2017.** Lossy image compression with compressive
434 autoencoders. *In Proc. Int. Conf. Learn. Representations*.1-19.
- 435 **L. Wang, Y. Wang, Q. Chang. 2016.** Feature selection methods for big data bioinformatics: A
436 survey from the search perspective. *Methods* **111**:21-31.
- 437 **Marco Capó, Aritz Pérez, Jose A. Lozano. 2021.** A Cheap Feature Selection Approach for the
438 K-Means Algorithm. *IEEE Transactions on Neural Networks and Learning Systems* **32(5)**:
439 2195-2208
- 440 **Mariucci E, Reiß M. 2017.** Wasserstein and total variation distance between marginals of Levy
441 processes. *ArXiv*:1710.02715.
- 442 **M. Luo, F. Nie, X. Chang. 2018.** Adaptive Unsupervised Feature Selection With Structure
443 Regularization. *IEEE Transactions Neural Network. Learning System* **29(4)**:944-956.
- 444 **Na Lei, Kehua Su, Li Cui. 2019.** A geometric view of optimal transportation and generative
445 model. *Computer Aided Geometric Design* **68**:1-28.
- 446 **P. Zadeh, R. Hosseini, S. Sra. 2016.** Geometric mean metric learning. *In Proc. Int. Conf. Mach.*
447 *Learning*. 2464- 2471.
- 448 **R. Hettiarachchi, J. F. Peters. 2015.** Multi-manifold lle learning in pattern recognition. *Pattern*
449 *Recognition* **48(9)**:2947-2960.
- 450 **R. Abadía-Heredia, M. López-Martín, B. Carro, J.I. Arribas, J.M. Pérez, S. Le Clainche.**
451 **2022.** A predictive hybrid reduced order model based on proper orthogonal decomposition
452 combined with deep learning architectures. *Expert Systems with Applications* **187**:1-15.
- 453 **Rami Al-Hmouz, Witold Pedrycz, Abdullah Balamash. 2022.** Logic-Oriented Autoencoders
454 and Granular Logic Autoencoders: Developing Interpretable Data Representation. *IEEE*
455 *Transactions on Fuzzy Systems* **30(3)**:869-877.
- 456 **R. Chakraborty, N. R. Pal. 2015.** Feature Selection Using a Neural Framework With
457 Controlled Redundancy. *IEEE Transactions Neural Network Learning System* **26(1)**:35-50.
- 458 **R. De Maesschalck, D. Jouan-Rimbaud, D. L. Massart. 2000.** The Mahalanobis distance,
459 Chemometrics Intell. Lab. System **50(1)**:1-18.
- 460 **S. Ying, Z. Wen, J. Shi. 2018.** Manifold preserving: An intrinsic approach for semisupervised
461 distance metric learning. *IEEE Transaction. Neural Networks Learning System* **29(7)**:
462 2731-2742.
- 463 **T. X. Pham, P. Siarry, H. Oulhadj. 2019.** A multi-objective optimization approach for brain
464 MRI segmentation using fuzzy entropy clustering and region-based active contour methods.
465 *Magn. Reson. Image* **61**:41-65.
- 466 **Ugochukwu Ejike Akpudo, Jang-Wook Hur. 2020.** Intelligent Solenoid Pump Fault Detection
467 based on MFCC Features, LLE and SVM. *2020 International Conference on Artificial*
468 *Intelligence in Information and Communication (ICAIC)*. 1-3.

- 469 **Weining Lu, Yu Cheng, Cao Xiao. 2017.** Unsupervised Sequential Outlier Detection with Deep
470 Architectures. *IEEE Transactions on Image Processing* **26(9)**:4321-4330.
- 471 **Xue, B., Zhang, M., Browne. 2015.** A Survey on Evolutionary Computation Approaches to
472 Feature Selection. *IEEE Transactions on Evolutionary Computation* **20(4)**:606-626.
- 473 **Zhiqiang Wan, Haibo He, Bo Tang. 2018.** A Generative Model for Sparse Hyperparameter
474 Determination. *IEEE Transactions on Big Data* **4(1)**:2-10.

Figure 1

The structure of the proposed m-AE

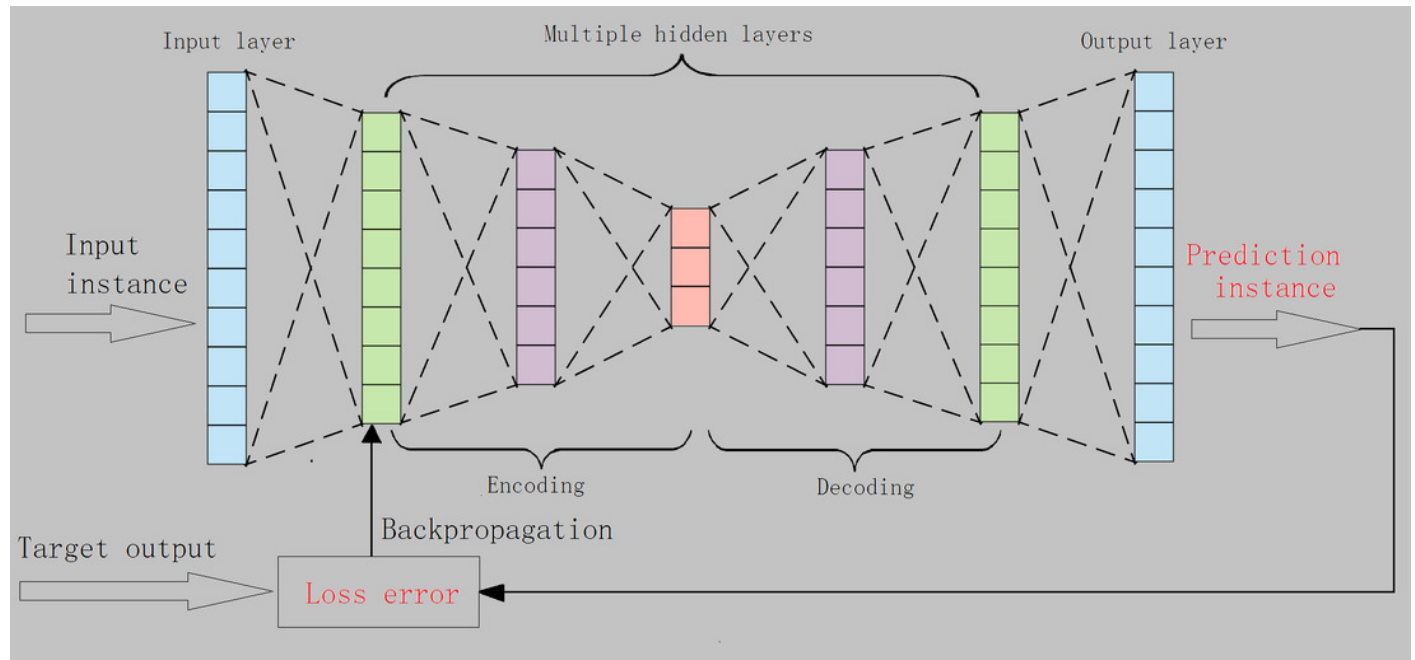
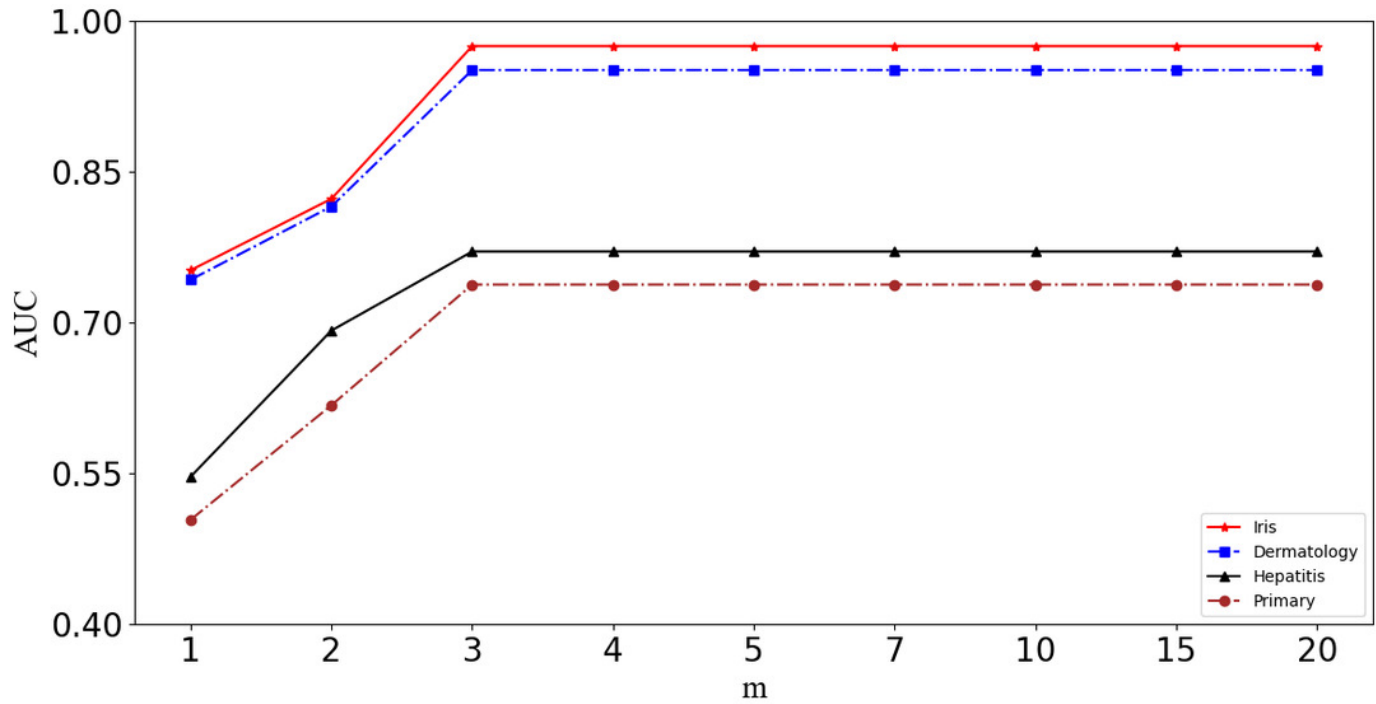
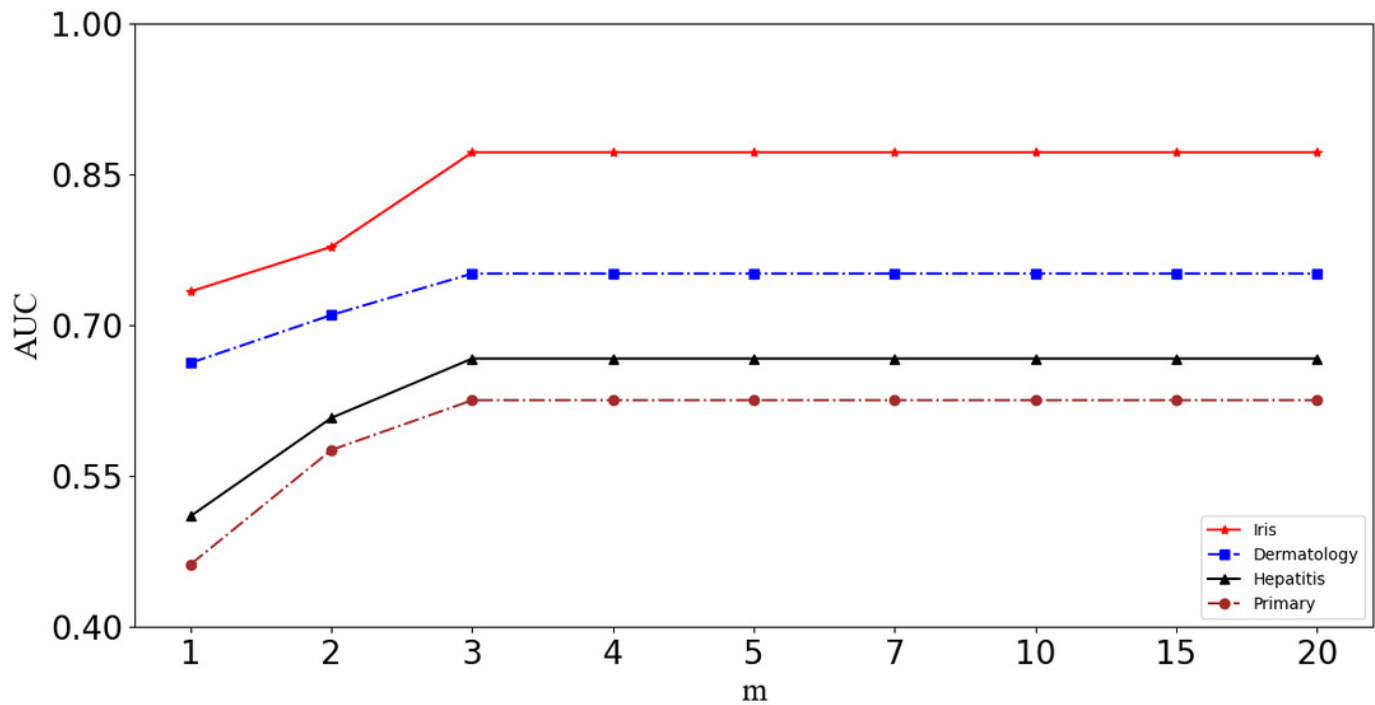


Figure 2

Validation of robustness



(a) m-AE



(b) AE-BK

Figure 3

Results of ablation experiments

(a) Comparisons between using distance metrics and without using distance metrics. These models using distance metrics are marked as the symbol \checkmark . The models without both distance metrics and feature selection are marked as the symbol \times . (b) Comparisons between using distance metrics and using feature selection. These models using feature selection are marked as the symbol \neq .

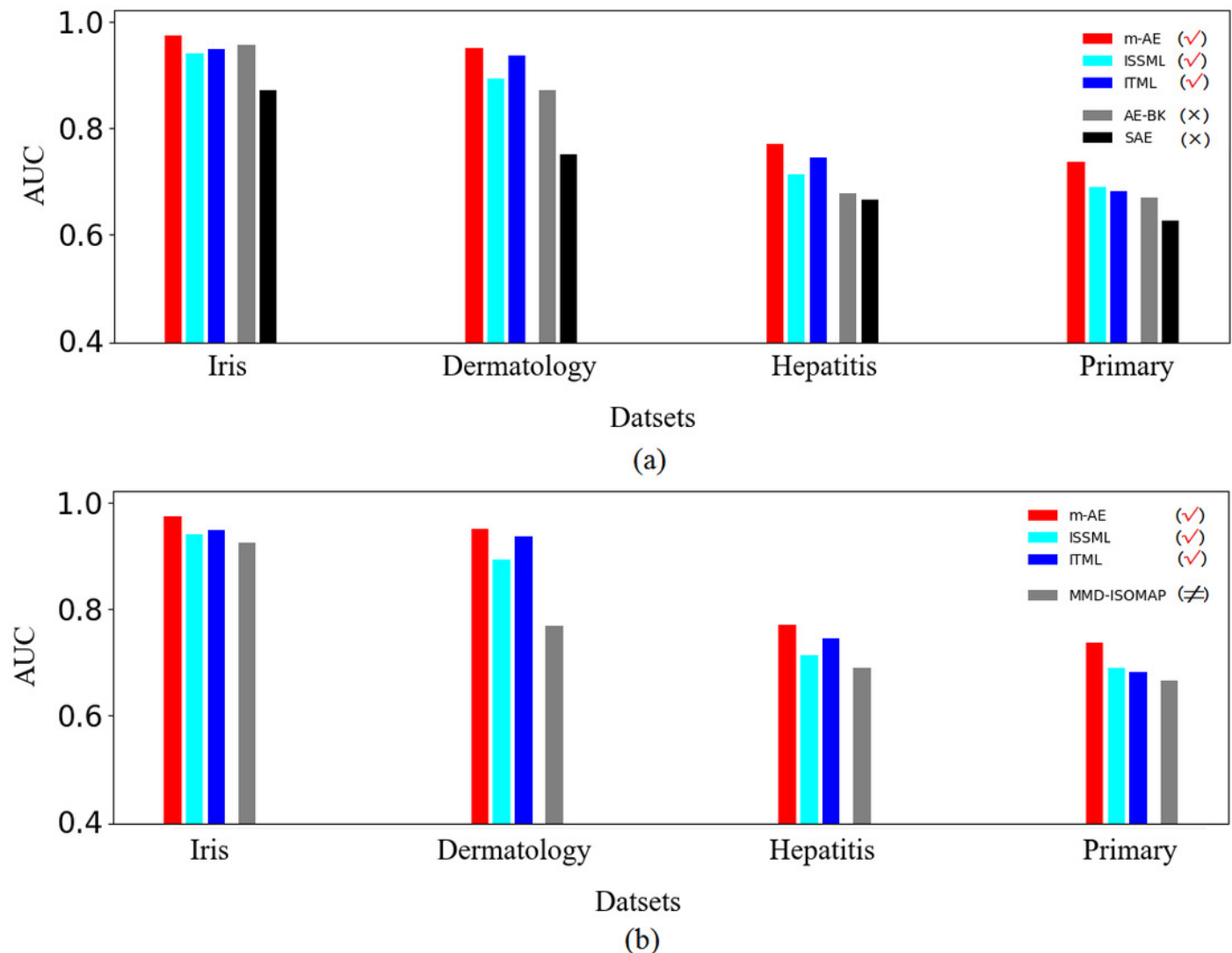


Figure 4

Visualization distributions.

The four datasets are Iris, Dermatology, Hepatitis, Primary from left to right, respectively. The different extracted features are marked with different shapes and colors. The models using distance metrics are marked as the symbol \checkmark . The models using feature selection are marked as the symbol \neq . The models without both distance metrics and feature selection are marked as the symbol \times .

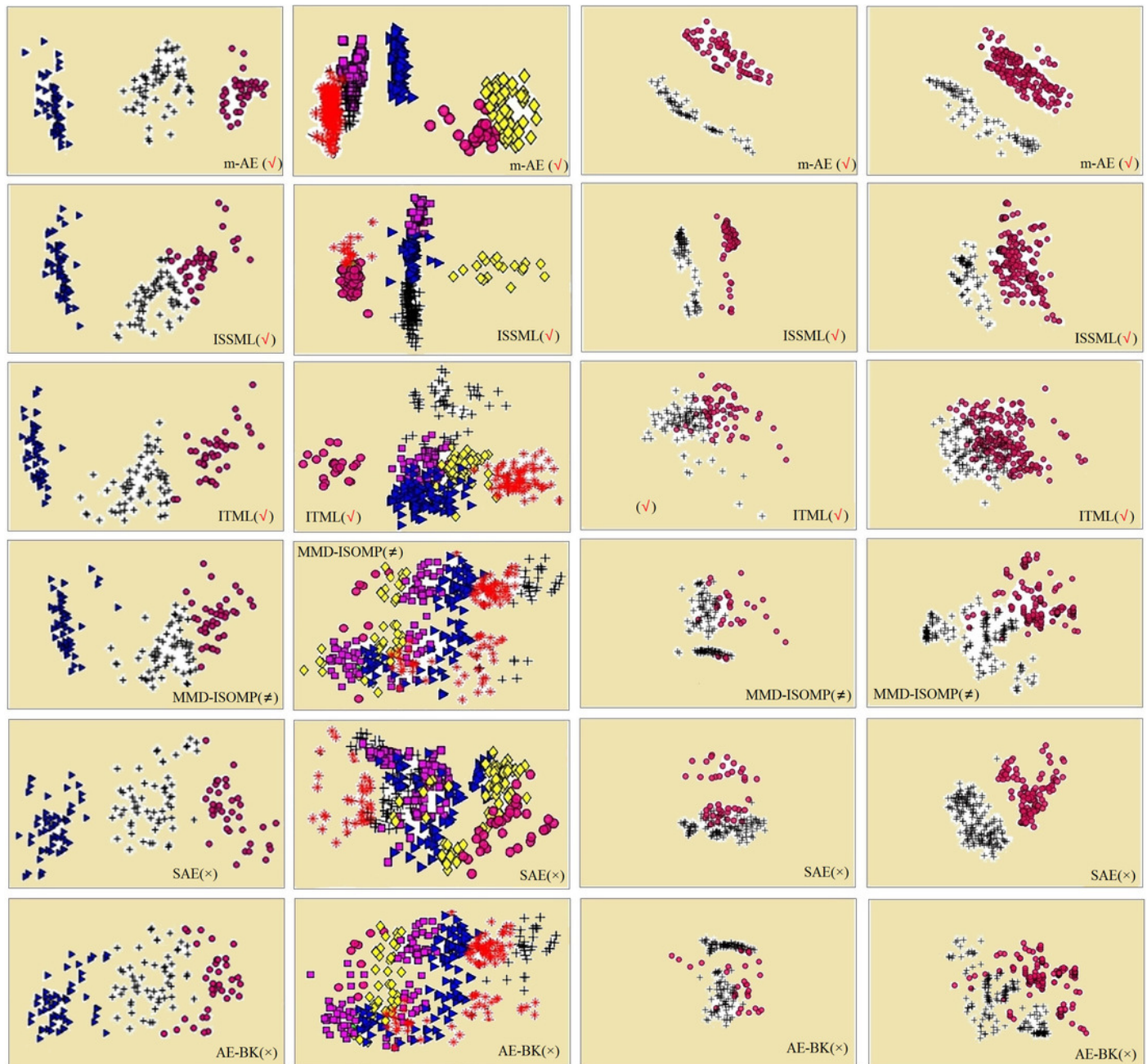


Figure 5

Runtime on benchmark datasets.

The models using distance metrics are marked as the symbol \checkmark . The models using feature selection are marked as the symbol \neq . The models without both distance metrics and feature selection are marked as the symbol \times .

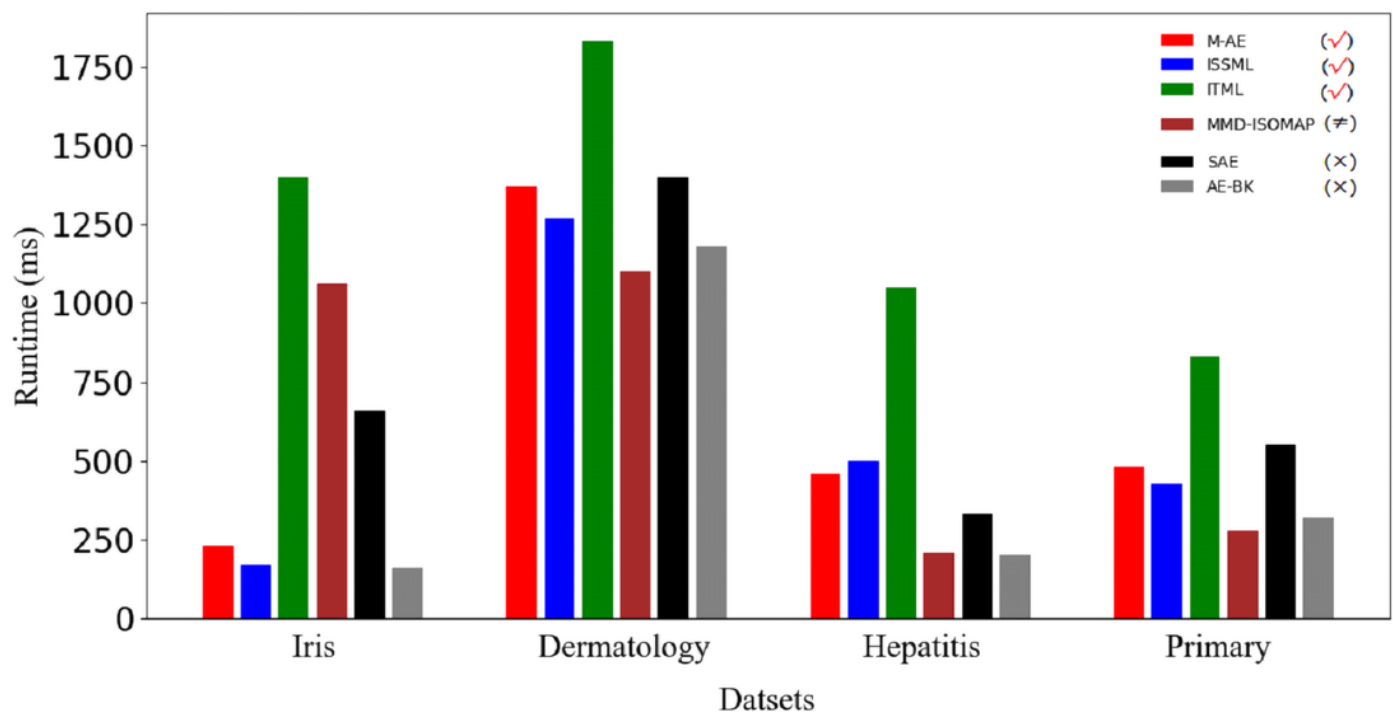


Table 1 (on next page)

Benchmark datasets

1

Dataset	Data volume	Data dimensionality	features
Iris	150	4	3
Primary	339	17	2
Hepatitis	155	19	2
Dermatology	366	33	6

2

Table 2 (on next page)

Accuracy of feature extraction.

The best accuracy for each dataset is shown in bold. The models using a distance metric are marked as the symbol \checkmark . The models using feature selection are marked as the symbol \neq .

The models without both a distance metric and feature selection are marked as the symbol \times .

1

		Iris	Dermatology	Hepatitis	Primary
m-AE	(✓)	0.9744 ±	0.9506 ±	0.7703 ±	0.7375 ±
		0.0157	0.0137	0.0753	0.0534
ISSML	(✓)	0.9402 ±	0.8931 ±	0.7131 ±	0.6886 ±
		0.0154	0.0284	0.0642	0.0865
ITML	(✓)	0.9488 ±	0.9374 ±	0.7457 ±	0.6816 ±
		0.0120	0.0246	0.0622	0.0745
MMD-ISOMAP		0.9247 ±	0.7680 ±	0.6897 ±	0.6664 ±
(≠)		0.0053	0.0377	0.0657	0.0733
SAE	(×)	0.9571 ±	0.8707 ±	0.6773 ±	0.6700 ±
		0.0227	0.0892	0.0373	0.0166
AE-BK	(×)	0.8715 ±	0.7511 ±	0.6666 ±	0.6252 ±
		0.1533	0.0099	0.0771	0.1052

2